J. Adv. Model. Earth Syst., **Vol. 1**, Art. #7, 11 pp.

Subtropical Low Cloud Response to a Warmer Climate in a Superparameterized Climate Model. Part I: Regime Sorting and Physical Mechanisms

Matthew C. Wyant, Christopher S. Bretherton and Peter N. Blossey

Department of Atmospheric Sciences, University of Washington, Seattle, Washington, USA

Manuscript submitted 19 March 2009; in final form 8 May 2009

The subtropical low cloud response to a climate with SST uniformly warmed by 2 K is analyzed in the SP-CAM superparameterized climate model, in which each grid column is replaced by a two-dimensional cloud-resolving model (CRM). Intriguingly, SP-CAM shows substantial low cloud increases over the subtropical oceans in the warmer climate. The paper aims to understand the mechanism for these increases. The subtropical low cloud increase is analyzed by sorting grid-column months of the climate model into composite cloud regimes using percentile ranges of lower tropospheric stability (LTS). LTS is observed to be well correlated to subtropical low cloud amount and boundary layer vertical structure. The low cloud increase in SP-CAM is attributed to boundary-layer destabilization due to increased clear-sky radiative cooling in the warmer climate. This drives more shallow cumulus convection and a moister boundary layer, inducing cloud increases and further increasing the radiative cooling. The boundary layer depth does not change substantially, due to compensation between increased radiative cooling (which promotes more turbulent mixing and boundary-layer deepening) and slight strengthening of the boundary-layer top inversion (which inhibits turbulent entrainment and promotes a shallower boundary layer). The widespread changes in low clouds do not appear to be driven by changes in mean subsidence.
In a companion paper we use column-mode CRM simulations based on LTS-composite profiles to further study the low cloud response mechanisms and to explore the sensitivity of low cloud response to grid resolution in SP-CAM.

DOI:10.3894/JAMES.2009.1.7

1. Introduction

Clouds play a large role in the climate system. Conventional atmospheric general circulation models (GCMs) parameterize unresolved cloud processes. Uncertainties in cloud parameterizations are a major factor in the overall uncertainty in climate model projections. Differences between models in the representation of low clouds have been identified as major cause of model disparity in climate response (Bony and Dufresne 2005). We do not yet have an accepted physical theory for predicting the response of low clouds to a climate change that allows us to prefer one GCM over another.

In most GCMs, multiple interacting parameterizations for turbulence, cloud fraction and microphysics, radiation, etc. determine low cloud properties. Although processes such as turbulence and condensation interact on the scale of individual updrafts and downdrafts, GCMs are forced to represent their interaction via parameterizations communicating on the much larger scale of a GCM grid cell, a challenging problem with no unique solution. Although the solutions to this problem embodied in different GCMs can be tested against current climate, this has so far provided little constraint on the GCMs' predictions of cloud feedbacks on future climate change.

CRMs can simulate turbulent cloud processes by using much finer spatial resolution than GCMs, but are typically run for shorter periods with much smaller domains due to their heavy computational requirements. The NICAM model (Tomita et al. 2005) is a global CRM. Because of its computational costs, only runs of seasonal duration are practical. Another approach is superparameterization (Grabowski 2001; Khairoutdinov and Randall 2001) in which a GCM is run with each grid column replaced by a CRM that interacts with the large-scale fields. With current implementations of either approach, boundary-layer clouds

To whom correspondence should be addressed.
Matthew C. Wyant, Department of Atmospheric Sciences, University of Washington, Seattle, WA 98195-1640, USA
mwyant@atmos.washington.edu

are severely under-resolved by the CRM grid. However, it may soon be computationally practical to use much higher resolution in the embedded CRMs of a superparameterization.

The focus of this paper is low-latitude boundary layer cloud response to a climate perturbation in the SP-CAM superparameterization (Khairoutdinov et al. 2005). SP-CAM uses the two-dimensional version of the System for Atmospheric Modeling (SAM, Khairoutdinov and Randall 2003) CRM embedded in each column of version 3.0 of the Community Atmosphere Model (CAM) GCM (Collins et al. 2006). CAM is run with 30 vertical levels and 2.8° x 2.8° horizontal grid spacing. The CRM replaces the cloud and moist-physics parameterizations within CAM. SP-CAM has 32 grid columns 4 km apart, aligned in the north-to-south direction, 28 vertical levels co-located with CAM model levels starting at the surface, and 2 fewer levels at the top of the domain. There are 9 levels between the surface and 700hPa. The specific version of SP-CAM used here is further described in Wyant et al. (2006a), hereafter referred to as W06.

W06 examined the cloud response of SP-CAM to a global 2K sea-surface temperature (SST) increase. This perturbation induced a significant increase in low cloud cover over the oceans in both the tropics and extra-tropics, implying strong negative cloud feedbacks on climate change. We focus on the cloud increases over the low latitude oceans (30S–30N; hereafter LLO) because the low clouds there vary less from day to day than in the extra-tropics, so they can be effectively analyzed using the monthly-mean fields for which we have SP-CAM model output.

Our goal in this paper is to use a cloud-regime binning approach to study the warming-induced LLO low cloud increase and its physical mechanism. In a companion paper (Blossey et al. 2009) we develop a CRM-based column analogue to SP-CAM that roughly matches its cloud climatology and cloud response to climate change in a typical trade-cumulus regime, with which we explore the sensitivity of the cloud response to the grid resolution of the embedded CRM.

Section 2 gives an overview of the SP-CAM low cloud climatology and its response to an SST increase. In Sect. 3, these are related to lower tropospheric stability (LTS), which is an empirical correlate of boundary-layer cloud amount in the current climate (Klein and Hartmann, 1993). In Sect. 4 we gain insight into the low cloud changes by compositing the LLO into cloud regimes using LTS percentile ranges. In Sect. 5, we use this analysis to propose a physical mechanism for the SP-CAM low cloud response. Section 6 presents our conclusions.

2. SP-CAM climatology and climate sensitivity

We analyze the two SP-CAM simulations presented in W06. The 3.67-year 'control' simulation uses climatological SST, and the 5.25-year '+2K' simulation is identical except that the SST is uniformly increased by 2K. Both control and +2K simulations use identical specified sea-ice climatologies. The simulations start on September 1 and the first 6 months of each simulation are discarded because of model spin-up. Monthly climatologies are created from the remainder of the simulations.

The global climate sensitivity, λ, can be calculated for this type of experiment based on the relation $\Delta T_s = \lambda G$, where ΔT_s is the global mean change in surface temperature and G is the change in net outgoing radiation (Cess et al. 1989). W06 found $\lambda = 0.67$ K m^2 W^{-1}, a low climate sensitivity when compare with other GCMs. This was attributed to increases in low cloud amount and liquid water path (LWP) at both low and high latitudes. These create a global mean change in net cloud forcing (NCF) of -1.77 W m^{-2} when SST is raised 2 K (NCF is defined as the difference between net downward radiative flux and the clear-sky net downward radiative flux at the top of the atmosphere. Shortwave cloud forcing (SWCF), used below, is defined analogously).

Figure 1a shows the annual mean low cloud fraction for the control run, defined as the integrated cloud fraction between the surface and 700hPa (This choice comfortably includes all marine boundary layer clouds).

Cloud fraction at a given level is defined as the fraction of horizontal grid points in the embedded CRM with condensed (liquid + ice) water content greater than 0.01 g kg^{-1} (This threshold is intended to exclude optically thin clouds from the definition). The realism of the SP-CAM low cloud distribution compares favorably with other contemporary GCMs but does have some notable deficiencies. The high stratocumulus amounts in the eastern subtropical oceans do not extend far enough westward. Much of the stratocumulus cloud near the coast reaches down to the surface, creating excessive fog-like stratocumulus.

The annual mean net cloud radiative forcing in SP-CAM is shown in Fig. 1b. The large negative NCF over high latitude oceans and subtropical stratocumulus regions are prominent, consistent with the large low-cloud fractions in these regions. Qualitatively the SP-CAM cloud forcing compares well with the annual mean ERBE (Earth Radiation Budget Experiment, Harrison et al. (1990)) net cloud forcing from the period 1986–1989 (Fig. 1c). However, the cloud forcing in the western oceans and the polar regions is too negative. Also, the 'stratocumulus' regions of strongly negative cloud forcing in the subtropics do not extend far enough westward away from the coasts.

On monthly timescales, low cloud amount has a strong space-time correlation with lower-tropospheric stability over the LLO (Klein and Hartmann 1993). LTS is conventionally defined as the difference between the potential temperature at 700 hPa and at 1000 hPa. For SP-CAM, we slightly modify this definition by replacing the temperature at 1000 hPa with the 2-m surface air temperature to minimize errors due to interpolation between model levels.

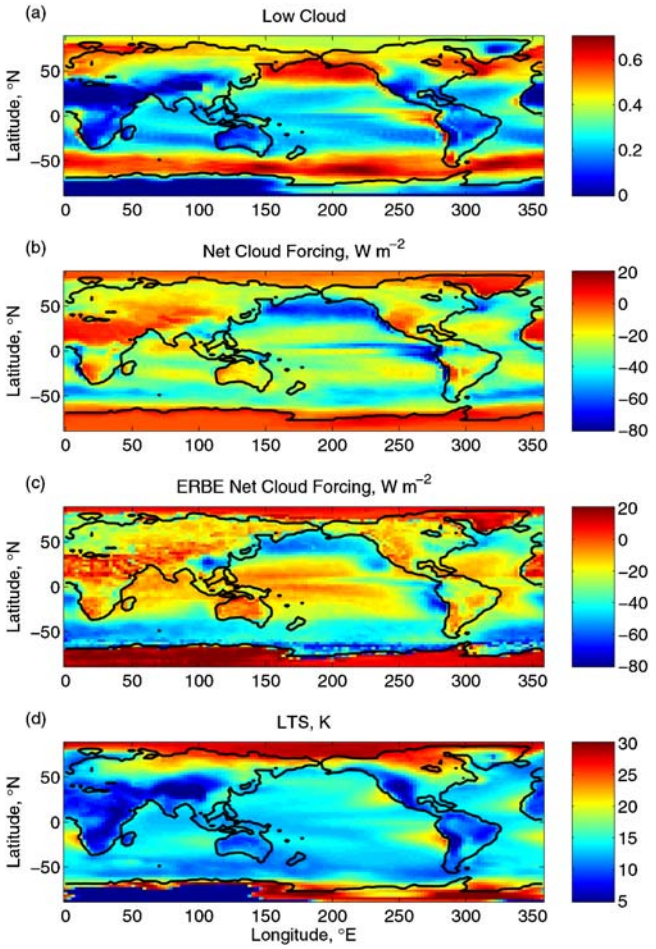

Figure 1. Annual mean SP-CAM fields and observations. (a) SP-CAM low cloud fraction in the control simulation, (b) SP-CAM net cloud forcing (W m^{-2}), (c) ERBE 1986–1989 net cloud forcing (W m^{-2}), and (d) SP-CAM lower tropospheric stability (K).

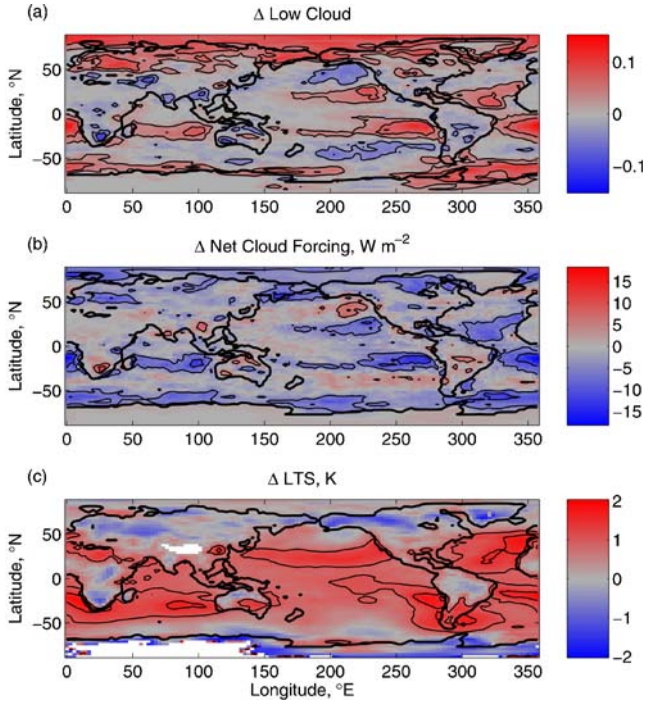

Figure 2. Changes in annual mean SP-CAM fields due to +2K SST increase. (a) Low cloud fraction (contours at −0.06, −0.03, 0.03, 0.06) , (b) net cloud forcing (contours at −10, −5, 5, and 10 W m^{-2}), and (c) LTS (contours at 1, 1.5 K).

The annual mean SP-CAM LTS is plotted in Fig. 1d. The spatial correlation between annual mean LTS and low cloud fraction over the LLO is 0.35 in SP-CAM. The observed annual correlation of low cloud amount from visual surface observations (Hahn and Warren 2007) and LTS from the European Centre for Medium-Range Weather Forecasting (ECMWF) 40-year reanalysis (ERA-40; Uppala et al. 2005) is 0.48. The positive correlation between LTS and maritime low cloud in SP-CAM is smaller at higher latitudes, as in observations.

Wood and Bretherton (2006) suggested a modification of LTS, the estimated inversion strength (EIS), that is a better predictor of mid-latitude maritime low clouds and which they speculated might be more applicable to prediction of climate-perturbation induced low cloud changes. We nevertheless use LTS in this paper because in SP-CAM and observations over the LLO, monthly-averaged LTS is somewhat better correlated with low clouds and NCF than is EIS. Furthermore, the statistical relationship between EIS and low cloud cover in SP-CAM shifts in the +2K climate, though to a lesser extent than with LTS. Hence, EIS does not prove to be a low cloud predictor that is invariant to climate perturbations, at least for SP-CAM.

3. LTS and climate sensitivity

The +2K low cloud increase in SP-CAM (Fig. 2a) is far from uniform, and induces a spatially anti-correlated change in net cloud forcing (Fig. 2b). Large regions of substantial low-cloud increases exceeding 0.03, with corresponding NCF changes of more than -5 W m^{-2}, are prominent in the cooler parts of the subtropical oceans. There are also substantial low cloud increases over broad regions at high latitudes. Smaller regions of decreased low cloud and increased NCF can be seen over low-latitude land and ocean storm-track regions.

Based on current climatology, we might hope that +2K changes in LTS would be a good predictor of changes in low cloud amount and NCF, at least over the LLO.

Indeed, along with the mean +2K increase of 2.3% in LLO low-cloud, there is a mean LTS increase of 1.03 K. However, geographic patterns of +2K LTS change (Fig. 2c) suggest a more complex picture. There are significant increases in LTS even in regions with no low cloud increase, such as the tropical west Pacific. These suggest a tendency for a given low cloud fraction to be associated with larger LTS in the warmer climate, as also seen in conventional GCM simulations by Medeiros et al. (2008). There is a clear geographical

correlation over the LLO (r = 0.59) between annual-mean changes in LTS and changes in low cloud. However, the regional variations of +2K LTS increase over the LLO are too small to be an attractive explanation of the large regional differences in low cloud change. The largest low cloud increases occur in subtropical belts, while the large increases in LTS occur poleward of these belts. Over land and at high latitudes the relationship between LTS changes and low cloud changes is less evident (and less expected). Hence, we do not regard the +2K changes in LTS as an adequate explanation of the +2K changes in low cloud cover and NCF. However, we do regard LTS as a useful analysis tool for low cloud changes, because it can efficiently sort the LLO into boundary-layer cloud regimes. This is explored in the next section.

4. Sorting by LTS

To understand the processes responsible for +2K subtropical oceanic low cloud increases, it is helpful to understand the typical changes in thermodynamic profiles that accompany them. We use a compositing approach to ensure our analysis is representative of the entire subtropics. LTS is a logical compositing variable because of its strong connection to observed low cloud amount and NCF. Compositing into LTS bins will sort the LLO into deep convection regions (low LTS), trade cumulus regions (intermediate LTS), and stratocumulus regions (high LTS). This approach follows Bony et al. (2004), but we choose LTS as a binning variable in place of monthly mean 500 hPa vertical velocity (or SST, which would be another plausible and simple choice) because it explains a significantly larger fraction of the observed space-time variance in monthly-mean NCF over the LLO.

For the climatology of each simulation, we calculate the LTS for each month at each grid point. Rather than sorting into bins with fixed LTS range, we sort each into 20 equally sized LTS bins. This sidesteps complications associated with the overall ~1 degree tropics-wide increase in LTS associated with the change of the moist adiabatic temperature profile in a warmer climate. Another advantage of this approach is its insensitivity to our choice of LTS as the stability metric. A similar analysis based on percentiles of a different stability measure, e. g. EIS or on the difference of SST from its tropical mean, would give almost indistinguishable results because the space/time structures of these stability metrics over the LLO are extremely highly correlated with that of LTS.

Figure 3 shows bin-means of low and total cloud fraction, low cloud frequency, net cloud forcing, and updraft cumulus mass flux (in buoyant saturated updrafts > 1 m s^{-1}) at 800 hPa, plotted against bin-mean LTS. Observed data sorted using LTS from ECMWF ERA-40 are plotted in Figures 3a, 3b and 3c as dotted lines. The bin-mean values of SP-CAM total cloud fraction only range from 0.30 to 0.41 across LTS bins. Above an LTS of 15K the low cloud amount increases with increasing LTS and dominates the total cloud fraction. The seasonal-mean observed low cloud fraction from Hahn and Warren (2007) has a very similar dependence on LTS, but is typically more than 0.2 larger than SP-CAM. This discrepancy could be partially due to the different methods of determining low cloud fraction between observation and model. The discrepancy is not as large when we compare observations from ISCCP (International Satellite Cloud Climatology Project; Rossow and Schiffer, 1999) and ISCCP simulator (Klein and Jakob, 1999) output from SP-CAM (Fig 3b). We use a monthly climatology of ISSCP D1 data from 1983–2001. We plot the frequency that highest cloud-top lies below 680hPa, regardless of cloud thickness, sorted by ERA-40 LTS. SP-CAM low cloud frequency is still much lower than observations at high LTS but within 0.1 of observations for most LTS bins.

The LTS binning preserves the geographical anti-correlation of SP-CAM net cloud forcing with the low cloud fraction. The ERBE net-cloud forcing is 10-20 W m^{-2} less negative than SP-CAM, though with broadly similar LTS dependence. Figure 3d shows that low LTS regions have high mean cumulus mass flux, corresponding to frequent strong deep convection, while high LTS regions have much less frequent and shallower convection.

Error bars in Figures 3a and 3c show the considerable scatter in low cloud and net cloud forcing in SP-CAM within bin populations representing the variability of many factors other than LTS including horizontal advection, vertical velocity, and absolute temperature. These variations are more pronounced as we move towards columns with higher LTS. These high LTS columns tend to be closer to the continents, where particular geographical features can play a large role in determining forcing. The significant variability in general within LTS bins should be borne in mind when considering LTS-composited mean quantities which are presented throughout this paper.

Figure 4a–d shows LTS-composited mean vertical profiles of cloud fraction, pressure velocity ω, relative humidity, and radiative heating rate. There is extensive deep convective and cirrus cloud, strong mean ascent, and high humidity through the entire troposphere in the weak LTS (warm SST) regions and mean subsidence, little mid and upper-level cloud, and a dry mid-troposphere in the strong LTS regions. Shallow trade-cumulus-like cloudiness maximizing around 900 hPa is present across all LTS bins, but increases at high LTS. At the highest LTS, the 'boundary layer' of extensive low cloud and high humidity becomes shallower, resembling fog. Especially for high LTS, there is strong radiative cooling (~2.5 K day^{-1}) in the humid, cloudy air in the upper parts of boundary layer, which helps destabilize it to convection.

We now investigate the +2K LLO cloud response of SP-CAM by applying similar LTS-percentile sorting to the +2K simulation and comparing the sorted results to the control simulation. The change in each variable of interest for a given percentile bin is calculated as the difference between

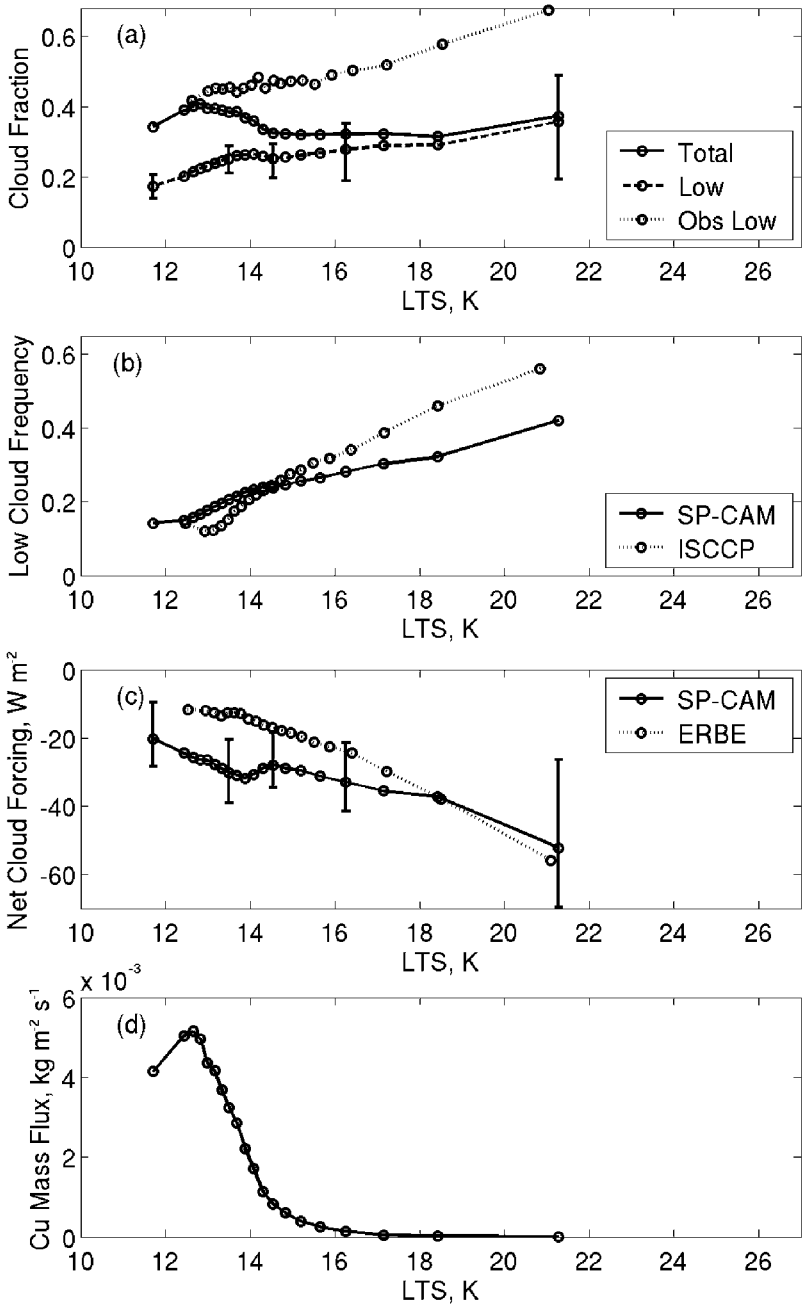

Figure 3. LTS-sorted mean SP-CAM fields from the control run and observations. (a) SP-CAM total cloud fraction (solid line), low cloud fraction (long dashed line) and observed seasonal-mean Hahn and Warren (2007) low cloud fraction (dotted line). (b) Low cloud frequency for SP-CAM using the ISCCP simulator (solid line) and ISCCP D1 data (dotted line). (c) Net cloud forcing in SP-CAM (solid, W m^{-2}) and ERBE (dotted) and (d) SP-CAM upwards cumulus mass flux (kg m^{-2} s^{-1}) versus bin-mean LTS. Each symbol represents one 5% bin of column-months. Error bars indicate 25th and 75th distribution percentiles for selected LTS bins for SP-CAM.

the bin-mean value for the +2K simulation and that for the control run. In the +2K simulation, bin-mean low cloud fraction increases in all tropical LTS bins (dotted line in Fig. 5a), though the largest increases occur in the highest LTS bins. These low cloud changes dominate the changes in total cloud fraction. There is mean negative NCF change across almost all LTS bins; the changes are generally stronger with increasing LTS bin (Fig. 5b) due to the strong low cloud increases.

The increase in mean LTS in each bin is shown in Fig. 5c. The increase in LTS is larger for the higher LTS percentiles, tracking similar trends in NCF and low cloud fraction. In the higher LTS bins from about 14K to 18K (65–95 percentiles), for each 1 K increase in control-run LTS, the

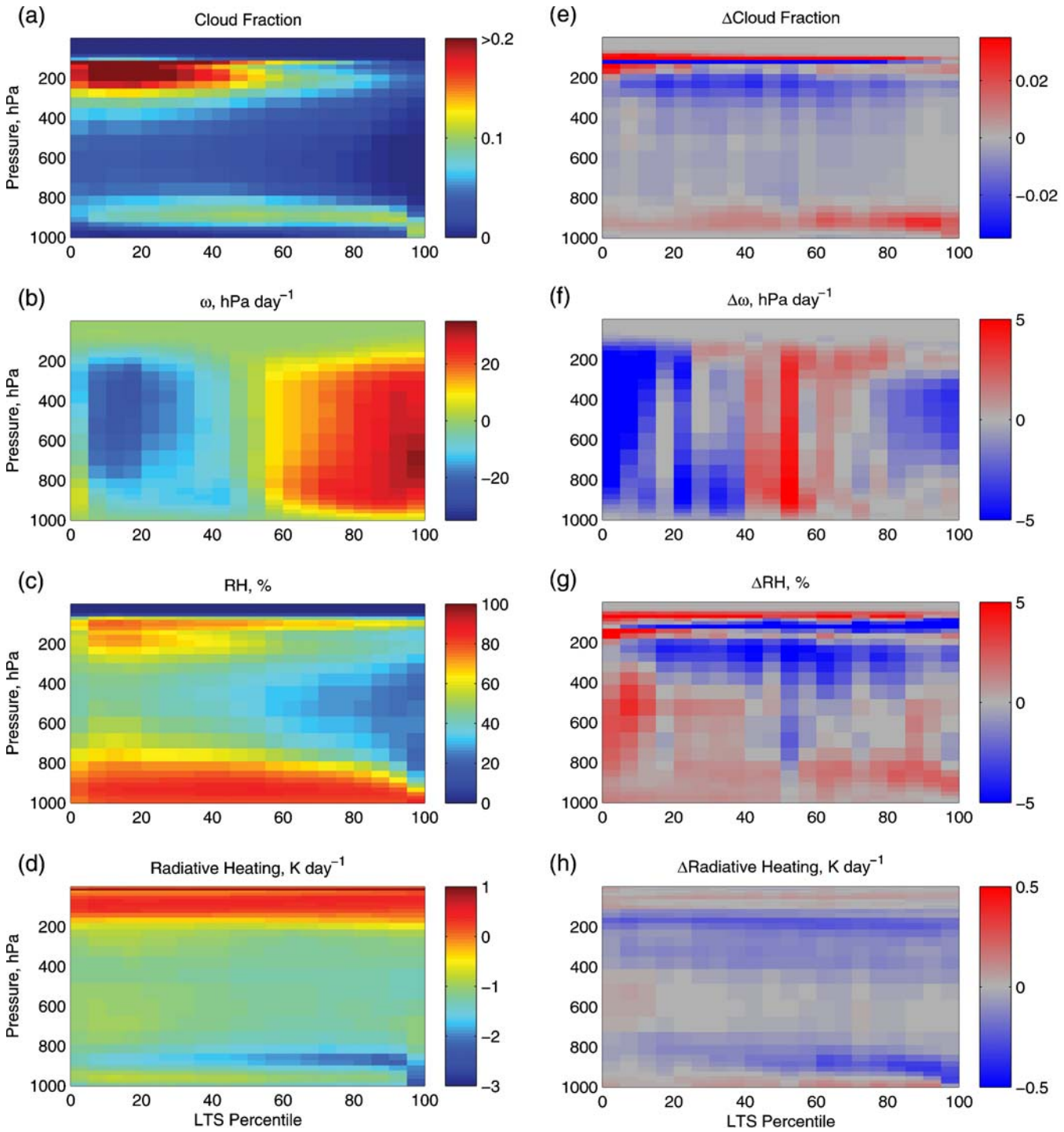

Figure 4. LTS-sorted mean vertical profiles for the SP-CAM control run. (a) cloud fraction, (b) pressure velocity (hPa day^{-1}), (c) relative humidity (%), and (d) radiative heating rate (K day^{-1}). LTS increases from left to right. In right column (e–h), the mean difference between the LTS-sorted +2K SST run and the control run is plotted for each variable (the color scale extrema are frequently exceeded in (e–h) in order to provide contrast for regions of interest).

SST+2K simulations exhibit an additional increase of 0.07 K in LTS, 0.01 in low cloud fraction, and -1.4 W m^{-2} in NCF. One might conclude that the large increase in low cloud in the high-LTS regimes is due to strengthening of the trade inversion. However, the implied sensitivity of low cloud fraction to LTS in this regime (0.035 for a 1 K LTS increase) is much stronger than the sensitivity of the control run low cloud fraction to control run LTS (from Figure 3, this is

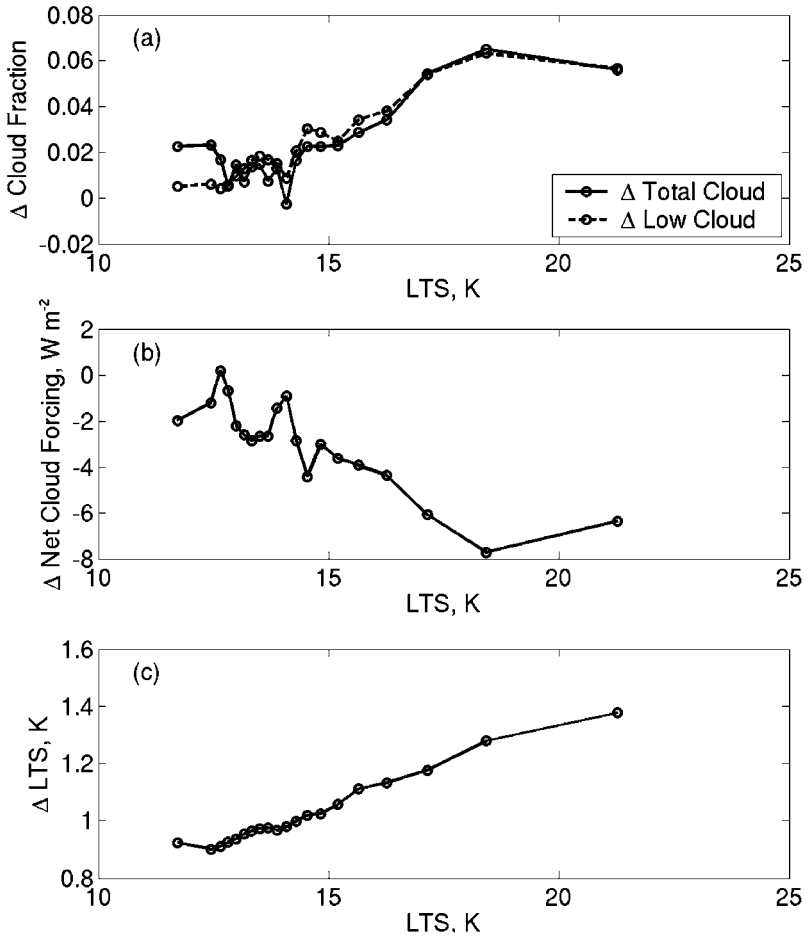

Figure 5. LTS-sorted changes in SP-CAM. (a) Change in total cloud fraction (solid) and low cloud fraction (dashed), (b) change in net cloud forcing (W m^{-2}), and (c) change in LTS (K) versus bin-mean control LTS.

about 0.01 per 1K LTS increase). This suggests that there is more to the +2K cloudiness changes than changes in inversion stability.

The vertical structure of the low cloud changes is shown in Fig. 4e. For most LTS bins the low cloud increases most at the level with the highest cloud fraction (The dipole pattern in high clouds is due to tropopause deepening caused by the +2K change). The total condensed liquid water content (not shown) increases roughly proportionally to the cloud fraction increases in the shallow clouds. Thus the mean in-cloud liquid water contents of these clouds are not appreciably different in the perturbed climate, in contrast to the cloud feedback mechanism proposed by Somerville and Remer (1984).

The LTS-sorted vertical velocity changes are more varied (Fig. 4f). For high LTS columns, the mean mid-tropospheric subsidence weakens, while near the surface, subsidence stays nearly constant. For moderate LTS columns, where the control vertical velocity is weak, subsidence is strengthened. For weak LTS, where deep convection is concentrated, the mean ascent is strengthened. The low

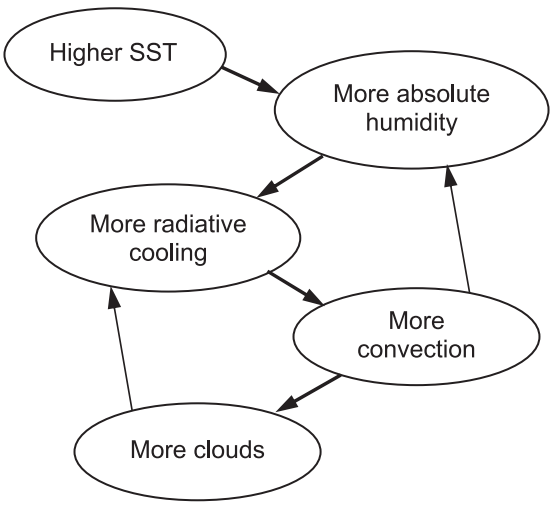

Figure 6. Schematic of hypothesized SP-CAM +2K low cloud response mechanism.

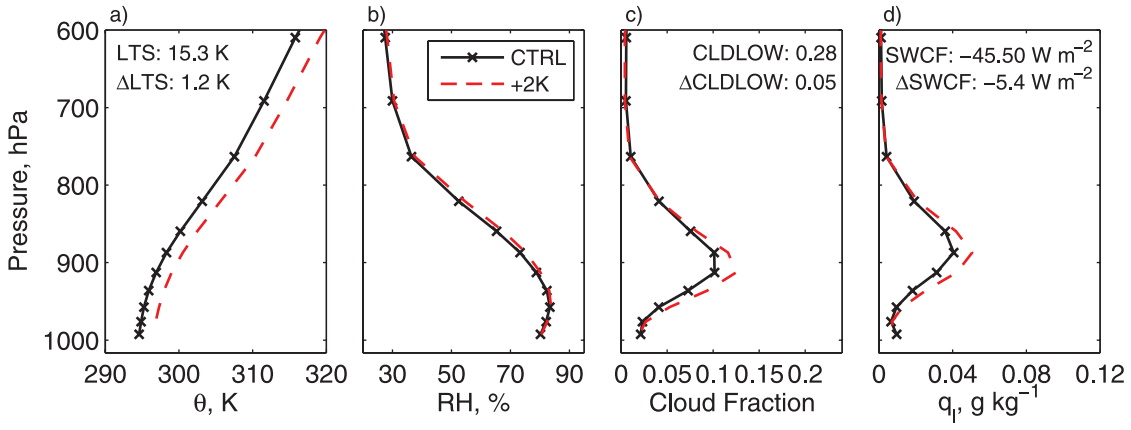

Figure 7. LTS80-90 mean vertical profiles. Both control run (black, solid) and +2K SST runs (red, dashed) are plotted. (a) potential temperature (K), (b) relative humidity (%) , (c) cloud fraction, and (d) cloud liquid water content (g kg^{-1}). The mean values of LTS, low cloud fraction (CLDLOW) and shortwave cloud forcing (SWCF) in the control run and their changes from the control to the +2K run are shown in panels, (a), (c) and (d), respectively.

cloud increases occur across all LTS categories, and do not appear to be strongly correlated to these ω changes.

In the moderate and high LTS columns, the relative humidity increases by 2 or 3% between about 800hPa and 900hPa (Fig. 4g). This increase is centered just above the levels of the largest cloud fraction increase. The radiative cooling also strengthens in these same regions by 0.2–0.4 K day^{-1} (Fig. 4h). Both of these changes are well correlated with the low cloud amount changes.

5. Mechanism of SP-CAM +2K low cloud response

There is little published work convincingly relating the LLO boundary layer cloud response of a GCM to a climate change to a particular physical mechanism operating in that model. Hypothesized physical mechanisms for cloud responses to climate change could be an important organizing tool for testing, analyzing and comparing GCMs, including sharper comparison with observations.

SP-CAM shows exceptionally large +2K increases in low cloud cover across the subtropics compared to most conventional GCMs. Furthermore, it relies on a CRM (albeit under-resolved) rather than purely a set of interacting physical parameterizations to produce this response. Hence, it seems worthwhile to try to rationalize the low cloud increases in SP-CAM.

In this section, we argue for the following novel radiatively-driven mechanism for this increase, diagrammed in Fig. 6. Higher SST causes a warmer and moister trade-cumulus boundary layer which experiences stronger net radiative cooling. The stronger cooling destabilizes the cumulus layer, leading to more vigorous convection. This fosters a moister boundary layer with more cumulus clouds, which amplifies the anomalous radiative cooling.

The overall +2K increase in lower tropospheric stability may help support this mechanism by keeping the more vigorous convection from enhancing penetrative entrainment of dry air that might evaporate cloud.

We have two pieces of indirect evidence for this mechanism. First, off-line radiation calculations show that even without any cloud or relative humidity increase, the +2K boundary layer would experience significantly stronger radiative cooling. For example, consider the 'LTS80-90' composite behavior over the 80–90 percentiles of LTS, chosen as a representative boundary-layer cloud regime with strong low cloud increases, minimal high-cloud effects, and no unrealistic fog. Figure 7 shows the LTS80-90 vertical profiles of θ, relative humidity (RH), cloud cover and cloud liquid water content for the control and +2K runs. These clearly show the +2K increases in boundary-layer cloud cover and liquid water content, the slight RH increase in the upper boundary layer. The inversion is slightly strengthened, contributing to increased LTS. Figure 8 compares the LTS80-90 composite control and +2K radiative heating profiles (thick lines) with offline calculations of the corresponding clear sky heating rate using LTS80-90 composite temperature and relative humidity profiles and SST (thin lines). The clear-sky radiative cooling in the perturbed climate is 0.1–0.25 K day^{-1} stronger than in the control climate throughout most of the cloud layer. This accounts for more than half the overall radiative cooling increase in the cloud layer. The slight +2K RH increase (Fig. 7b) has little impact on the clear-sky cooling. This can be seen by computing the latter using the +2K temperature profile but RH from the control climate (chain-dashed line in Fig. 8). Instead, the +2K clear-sky cooling increase is driven by the large boundary-layer specific humidity increase due to the warmer temperature profile. The remaining increase in the +2K radiative cooling increase is due to increased low cloud.

A second line of evidence supporting our hypothesized mechanism for low cloud increase comes from diagnosing

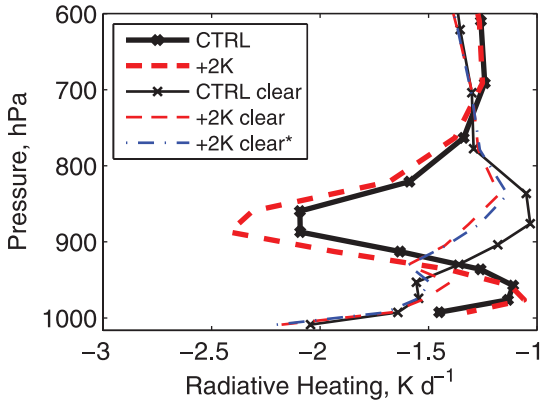

Figure 8. Vertical profiles of diurnal-mean radiative heating rate for LTS80-90. Full-sky SP-CAM (thick) calculated clear-sky (thin) profiles are plotted for the control run (black, solid) and the +2K SST run (red, dashed). An additional clear-sky profile from the +2K case is calculated (blue chain-dashed line) that uses the RH profile from the control case.

the monthly-mean net convective heating Q_{1c} in SP-CAM, which we interpret as a measure of the intensity of moist convection. Q_{1c} was calculated as a residual in the SP-CAM heat budget, as we now explain. SP-CAM and SAM use moist-conserved prognostic variables, the liquid-ice static energy $s_{li} = c_pT + gz - L(q_l + q_i) - L_f q_i$ and the total water $q_t = q_v + q_l + q_i$. Here T is temperature, and q_v, q_l and q_i are the mixing ratios of water vapor, liquid, and ice.

L and L_f are the latent heats of condensation and freezing, respectively. In each SP-CAM grid column (i.e. horizontally-averaged across the CRM simulating that grid column) the budget equations of s_{li} and q_t can be written:

$$\frac{\partial s_{li}}{\partial t} = c_p Q_1 - (\mathbf{u}\cdot\nabla s_{li})_h - \omega\frac{\partial s_{li}}{\partial p} \quad (1)$$

$$\frac{\partial q_t}{\partial t} = Q_{qt} - (\mathbf{u}\cdot\nabla q_t)_h - \omega\frac{\partial q_t}{\partial p} \quad (2)$$

Here Q_1 is the diabatic heating, composed of radiative heating Q_R and convective/turbulent heating Q_{1c}, while Q_{qt} is the diabatic moistening. The other terms on the right hand side are the large-scale horizontal and vertical advective heat and moisture tendencies.

The monthly averages of the total (vertical + horizontal) advective heat and moisture tendencies used to force the CRM in each grid column were saved in the SP-CAM simulations. These include the rectified effect of transients. The composite heat storage is very small, so the LTS-composited diabatic heating rate $Q_1(p)$ must balance the composite advective heating (and similarly for moisture). The convective heating Q_{1c} is inferred by subtracting the composite radiative cooling rate $Q_R(p)$ (Fig. 8) from $Q_1(p)$.

Figure 9 shows the LTS-binned profiles of composite Q_{1c} for the control simulation and their change from the control to the +2K simulation. The +2K simulation has 0.2 K (10%) stronger convective heating at 900 hPa for LTS80-90, the same level as the maximum cloud cover increase and just below the level of maximum radiative cooling increase. Similar results are seen in other high-LTS bins. This suggests in the +2K simulation that the cloud increases are associated with more convection.

Finally, the +2K boundary-layer changes have interesting interactions with the large-scale circulation. Within the cloud layer, up to half of the +2K radiative cooling increase (see Figs. 4h and 8) is compensated by more convective heating (Fig. 9b). The remaining cooling drives subsidence. Figure 10a shows the control and +2K LTS80-90 composite vertical motion. The weaker subsidence in the mid-troposphere (600 hPa) can be explained by examining the approximate heat balance. At that level, radiation dominates the diabatic cooling, but there is no radiative cooling change associated with the +2K change (Fig. 8). Since the +2K thermal stratification is stronger, weaker subsidence in the mid-troposphere is required to maintain heat balance.

In the cloud layer (900 hPa), strengthened diabatic cooling balances the stronger stratification and subsidence remains just as strong in the +2K climate. Subsidence is

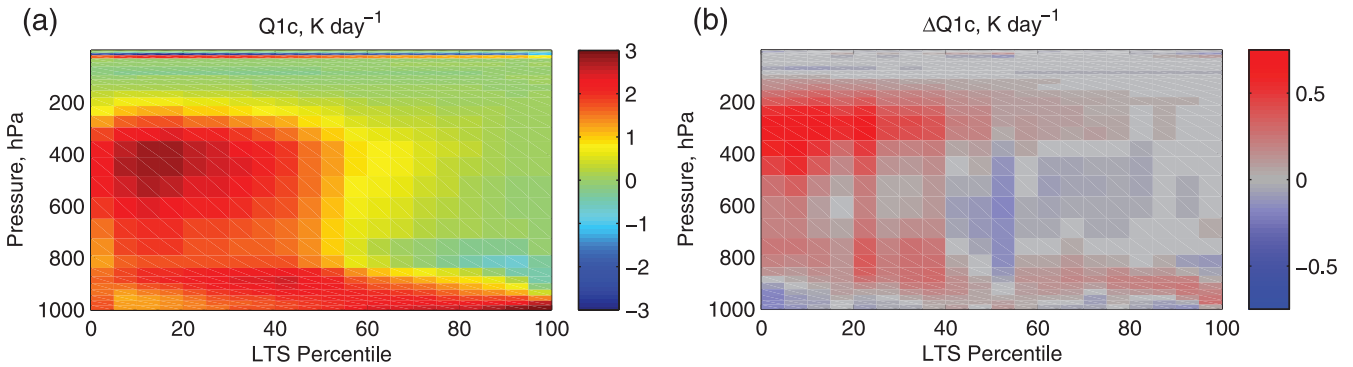

Figure 9 Monthly LTS-sorted profiles of convective heating Q_{1c} (K day^{-1}). (a) Control run and (b) the change from the control to the +2K SST simulation.

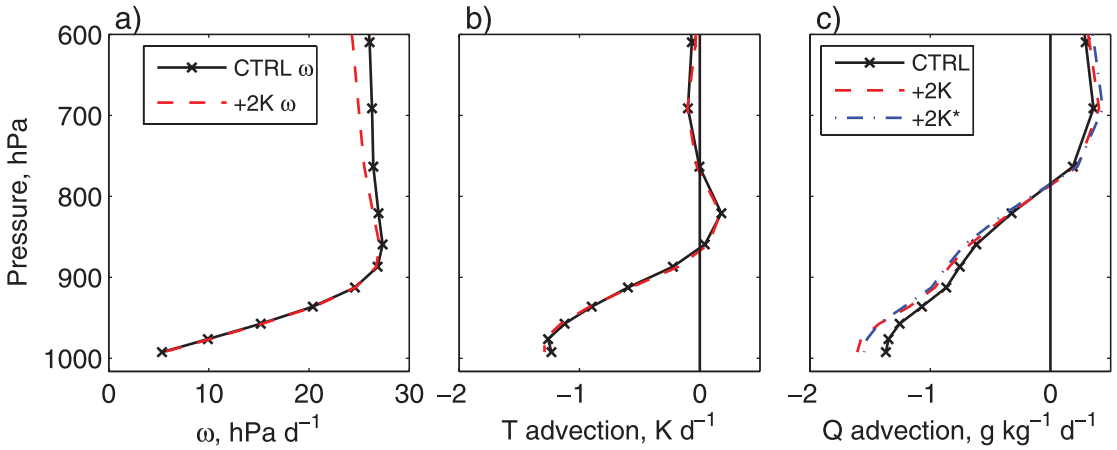

Figure 10. SP-CAM LTS80-90 composite profiles. Profiles are shown for SP-CAM control (black, solid) and the +2K simulation (red, dashed). (a) Pressure-velocity ω (hPa d^{-1}), (b) temperature advection (K d^{-1}), and (c) humidity advection (g kg^{-1} d^{-1}). The blue chain-dashed line in (c) is the horizontal humidity advection predicted for the +2K run if relative humidity from the control run is used.

viewed here as a feedback on the column diabatic processes rather than a fundamental external control.

Could changes in horizontal advection drive the cloud response? The dashed lines in Figs. 10b and 10c show the LTS80-90 horizontal advective forcing of temperature and specific humidity estimated as the difference between the composite SP-CAM total advective forcing and the vertical advective forcing. The horizontal advective heating profile (Fig. 10b) shows very little +2K change. Since these changes are small compared to the clear-sky radiative cooling changes (Fig 8, thin lines), they probably are not the main driver of the +2K SP-CAM low cloud increase.

The +2K increase in amplitude of the horizontal advective moistening (Fig. 10c), including stronger drying in the cloud layer and at the surface, is largely attributable to the Clausius-Clapeyron effect. When the +2K moisture advection is instead calculated using temperatures and winds from the +2K run but relative humidity fields from the control run (blue chain-dashed curve), the result is very similar to the original +2K moisture advection (red dashed curve). The +2K increase in advective drying also does not help explain the low cloud increase.

6. Discussion and conclusions

The SP-CAM exhibits large increases in low cloud cover in a climate in which SST is artificially warmed by 2 K. Much of this cloud increase occurs in subtropical marine boundary layers. Lower tropospheric stability (LTS) is used to analyze the cloud changes. In the Tropics, high LTS is closely correlated with cool SST. The overall tropical LTS increases by 1 K even in regions of no low cloud increase. Over the cooler subtropical oceans, there is a slightly larger LTS increase and a low cloud cover increase of over 5%.

We composited SP-CAM monthly-mean output from all oceanic low-latitude grid columns into climate regimes defined using percentiles of LTS. By comparing the SP-CAM control and +2K climates, we argued that the low cloud increase is ultimately driven by an increase in clear-sky radiative cooling in the relatively humid boundary layer air. This destabilizes the boundary layer, stimulating more convection, more cumulus cloud and further amplifying the radiative cooling. The vertical structure of the clouds shows little change in the warmer climate due to compensation between increased radiative destabilization of convection and inhibition of convective deepening by increased lower-tropospheric static stability. Horizontal advective forcing and boundary-layer winds are insensitive to the +2K forcing changes and appear to play little role in the SP-CAM cloud response.

We have taken a preliminary look at experiments using a few other GCMs to see the extent to which this mechanism may play a role in their low cloud changes. Like SP-CAM, the majority of models exhibit an increase in boundary layer radiative cooling for higher LTS bins with SST+2K. However the low cloud response in these models varies widely by model. The impact of SP-CAM vertical and horizontal resolution on this low cloud feedback is substantial (though it does not alter the sign of the low cloud response) and is further explored in Part II (Blossey et al. 2009).

The boundary-layer radiative feedbacks discussed here may also be quite sensitive to the type of climate perturbation. For instance, the increase in clear-sky boundary-layer radiative cooling in a climate warmed by doubled CO_2 might be rather weaker due to the system-wide radiative balance constraint. This might lead to much weaker cloud feedbacks than in the +2K case studied here. Conventional AGCMs often show rather different cloud responses to these two climate perturbations (e.g. Wyant et al. 2006b). Studying the response of SP-CAM to an instantaneous CO_2 increase with fixed SST could yield preliminary insights without the computational expense of a 20+ year simulation over a mixed-layer ocean (Gregory and Webb 2008).

Acknowledgements: This research was funded by NSF grant ATM 0425247 as part of the CMMAP Science and Technology Center. Marat Khairoutdinov performed the SP-CAM simulations that are the basis for this study. ERA-40 data was provided by ECMWF and NCAR DSS. ISCCP data was obtained from the Langley Distributed Active Archive Center.

References

Blossey, P., C. S. Bretherton, and M. C. Wyant, 2009: Subtropical low cloud response to a warmer climate in a superparameterized climate model. Part II: Column modeling with a cloud resolving model. *J. Adv. Model. Earth Systems*, **1**, Art. #8, 14 pp., doi: 10.3894/JAMES.2009.1.8.

Bony, S. and J. DuFresne, 2005: Marine boundary layer clouds at the heart of tropical cloud feedback uncertainties in climate models. *Geophys. Res. Lett.*, **32**, L20806, doi: 10.1029/2005GL023851.

Bony, S., J. DuFresne, H. Le Treut, J.-J. Morcrette, and C. Senior, 2004: On dynamic and thermodynamic components of cloud changes. *Climate Dyn.*, **22**, 71–86, doi: 10.1007/s00382-003-0369-6.

Cess, R. D. and 19 co-authors, 1989: Interpretation of cloud-climate feedback as produced by 14 atmospheric general circulation models. *Science*, **245**, 513–516, doi: 10.1126/science.245.4917.513.

Collins, W. D., P. J. Rasch, B. A. Boville, J. J. Hack, J. R. McCaa, D. L Williamson, B. P. Briegleb, C. M. Bitz, S.-J. Lin, and M. Zhang, 2006: The formulation and atmospheric simulation of the Community Atmospheric Model Version 3 (CAM3). *J. Climate*, **19**, 2144–2161, doi: 10.1175/JCLI3760.1.

Grabowski, W., 2001: Coupling cloud processes with the large scale dynamics using the cloud-resolving convective parameterization (CRCP). *J. Atmos. Sci.*, **58**, 978–997, doi: 10.1175/1520-0469(2001)058<0978:CCPWTL>2.0.CO;2.

Gregory, J., and M. Webb, 2008: Tropospheric adjustment induces a cloud component in CO2 forcing. *J. Climate*, **21**, 58–71, doi: 10.1175/2007JCLI1834.1.

Hahn, C.J., and S.G. Warren, 2007: *A Gridded Climatology of Clouds over Land (1971–96) and Ocean (1954–97) Worldwide*. NDP-026E, Carbon Dioxide Information Analysis Center, Oak Ridge National Laboratory, Oak Ridge, TN.

Harrison, E. F., P. Minnis, B. R. Barkstrom, V. Ramanathan, R. D Cess, and G. G. Gibson, 1990: Seasonal variation of cloud radiative forcing derived from the earth radiation budget experiment. *J. Geophys Res.*, **95**, 11679–11698, doi: 10.1029/JD095iD11p18687.

Khairoutdinov, M. F., and D. A. Randall, 2001: A cloud resolving model as a cloud parameterization in the NCAR community climate system model: Preliminary results. *Geophys. Res. Lett.*, **28**, 3617–3620, doi: 10.1029/2001GL013552.

Khairoutdinov, M. F., and D. A. Randall, 2003: Cloud resolving modeling of the ARM summer 1997 IOP: Model formulation, results, uncertainties, and sensitivities. *J. Atmos. Sci.*, **60**, 607–625, doi: 10.1175/1520-0469(2003)060<0607:CRMOTA>2.0.CO;2.

Khairoutdinov, M., D. Randall, and C. DeMott, 2005: Simulations of the atmospheric general circulation using a cloud-resolving model as a superparameterization of physical processes. *J. Atmos. Sci.*, **62**, 2136–2154, doi: 10.1175/JAS3453.1.

Klein, S., and D. Hartmann, 1993: The seasonal cycle of low stratiform clouds. *J. Climate*, **6**, 1587–1606, doi: 10.1175/1520-0442(1993)006<1587:TSCOLS>2.0.CO;2.

Klein, S., and C. Jakob, 1999: Validation and sensitivities of frontal clouds simulated by the ECMWF model. *Mon. Weather Rev.*, **125**, 2514–2531, doi: 10.1175/1520-0493(1999)127<2514:VASOFC>2.0.CO;2.

Medeiros, B., B. Stevens, I. M. Held, M. Zhao, D. L. Williamson, J. G. Olson, and C. S. Bretherton, 2008: Aquaplanets, climate sensitivity, and low clouds. *J. Climate*, **21**, 4974–4991, doi: 10.1175/2008JCLI1995.1.

Rossow W. B. and R. A. Schiffer 1999: Advances in understanding clouds from ISCCP. *Bull Am Meteor Soc.*, **80**, 2261–2287, doi: 10.1175/1520-0477(1999)080<2261:AIUCFI>2.0.CO;2.

Somerville, R. C. J. and L. A. Remer, 1984: Cloud optical thickness feedbacks in the CO_2 climate problem. *J. Geophys. Res.*, **89**, 9668–9672, doi: 10.1029/JD089iD06p09668.

Tomita, H., H. Miura, S. Iga, T. Nasuno, and M. Satoh, 2005: A global cloud-resolving simulation: Preliminary results from an aqua planet experiment. *Geophys. Res. Lett.*, **32**, L08805, doi: 10.1029/2005GL022459.

Uppala, S. M., and co-authors, 2005: The ERA-40 reanalysis. *Quart. J. Roy. Meteor. Soc.*, **131**, 2961–3012 doi: 10.1256/qj.04.176.

Wood, R., and C. S. Bretherton, 2006: On the relationship between stratiform low cloud cover and lower tropospheric stability. *J. Climate*, **19**, 6425–6432, doi: 10.1175/JCLI3988.1.

Wyant, M. C., M. Khairoutdinov, and C. S. Bretherton, 2006a: Climate sensitivity and cloud response of a GCM with a superparameterization. *Geophys. Res. Lett.*, **33**, L06714, doi: 10.1029/2005GL025464.

Wyant, M. C., C. S. Bretherton, J. T. Bacmeister, J. T. Kiehl, I. M. Held, M. Zhao, S. A. Klein, B. J. Soden, 2006b: A comparison of low-latitude cloud properties and responses in AGCMs sorted into regimes using mid-tropospheric vertical velocity. *Climate Dyn.*, **27**, 261–279, doi: 10.1007/s00382-006-0138-4.